Naval Research Laboratory
Washington, DC 20375-5000

NRL Memorandum Report 6774

Studies of Synchrotron Radiation Emission from the NRL Modified Betatron Accelerator*

T. J. SMITH, J. GOLDEN,† AND C. A. KAPETANAKOS

Beam Physics Branch
Plasma Physics Division

**Supported by ONR and SPAWAR*

†*Berkeley Research Associates*

January 24, 1991

REPORT DOCUMENTATION PAGE

Form Approved
OMB No 0704-0188

1. AGENCY USE ONLY *(Leave blank)*	2. REPORT DATE	3. REPORT TYPE AND DATES COVERED
	1991 January 24	Interim

4. TITLE AND SUBTITLE
Studies of Synchrotron Radiation Emission from the NRL Modified Betatron Accelerator*

5. FUNDING NUMBERS
TA RR011-09-41
WU 1485
TA XF-11133
WU 2835

6. AUTHOR(S)
T.J. Smith, J. Golden†, and C.A. Kapetanakos

7. PERFORMING ORGANIZATION NAME(S) AND ADDRESS(ES)
Naval Research Laboratory
Plasma Physics Division
Code 4795
Washington, DC

8. PERFORMING ORGANIZATION REPORT NUMBER
NRL Memorandum Report 6774

9. SPONSORING/MONITORING AGENCY NAME(S) AND ADDRESS(ES)
Office of Naval Research
Arlington, VA 22217-5000

10. SPONSORING/MONITORING AGENCY REPORT NUMBER

11. SUPPLEMENTARY NOTES
*Supported by ONR and SPAWAR.
†Berkeley Research Associates

12a. DISTRIBUTION/AVAILABILITY STATEMENT
Approved for public release; distribution unlimited.

12b. DISTRIBUTION CODE

13. ABSTRACT *(Maximum 200 words)*

Numerical calculations of synchrotron radiation emitted from the NRL modified betatron accelerator show that, for relativistic electron energies up to approximately 2 MeV, the single particle intensity spectrum is characterized by a peak at the Doppler-shifted cyclotron frequency associated with the applied toroidal field. Measurements of the radiation using fixed-frequency heterodyne receivers indicate that the polarization, amplitude, and the temporal evolution of radiated power during acceleration are in very good agreement with the predicted single particle spectrum. The observations have been used to confirm the energy evolution and provide information about the magnitude of the transverse velocity of the beam electrons for the first few hundred microseconds of acceleration. Late-time signal decay suggests that electrons are moving off the minor axis in a manner that is consistent with the excitation of the electron-cyclotron resonance.

14. SUBJECT TERMS
Synchrotron Radiation. Accelerator. Betatron. Heterodyne.

15. NUMBER OF PAGES
31

16 PRICE CODE

17. SECURITY CLASSIFICATION OF REPORT	18. SECURITY CLASSIFICATION OF THIS PAGE	19. SECURITY CLASSIFICATION OF ABSTRACT	20. LIMITATION OF ABSTRACT
UNCLASSIFIED	UNCLASSIFIED	UNCLASSIFIED	UL

CONTENTS

STUDIES OF SYNCHROTRON RADIATION EMISSION FROM THE NRL MODIFIED BETATRON ACCELERATOR*

I. Introduction

There has been considerable recent interest in the production of relativistic, multi-kiloampere electron beams for a variety of military and commercial applications. The need for high current, ultra-relativistic beam sources, as well as practical constraints on the size and weight of the devices required to generate these beams, has encouraged research in the development of compact, high current, induction accelerators.[1-5]

Among the most promising accelerator concepts is the modified betatron.[6-8] In contrast to the conventional betatron,[9,10] the magnetic field configuration of the modified betatron includes a strong toroidal guide field which permits stable equilibria for high current electron rings. Recently, experiments on the modified betatron accelerator (MBA) at the Naval Research Laboratory (NRL) have resulted in the acceleration of a 0.5 MeV, kiloampere beam to a terminal energy of approximately 18 MeV.[11]

Generic to the cyclic accelerators is the problem of obtaining information about the electron microstate without disrupting the ring equilibrium by repeated target interactions. Thompson backscattering has been used successfully to diagnose the energy spread of an intense relativistic electron beam.[12] However, this method requires higher current density and knowledge of the beam position with greater precision than is presently available in the MBA. Chernin and Levush[13] have proposed the use of synchrotron emission produced by betatron oscillations as a beam diagnostic technique. An investigation of the radiation fields that result from electron motion in the modified betatron field configura-

Manuscript approved November 5, 1990.
* Supported by ONR and SPAWAR

tion has revealed distinctive characteristics in the spectral signature and polarization.[13,14] Furthermore, synchrotron radiation has long been recognized as an important tool in the diagnosis of laboratory and space plasmas, because of the strong dependence of the spectral distribution on the motion of the individual-electrons. The subject has been treated extensively by a number of authors.[15–24] This paper describes the results of a numerical and experimental study of the synchrotron radiation emission from the NRL modified betatron accelerator. The focus of the study is the development of a technique for accurately predicting the radiation spectrum that results from the complex electron orbits, the experimental confirmation of the predicted spectrum, and the investigation of synchrotron radiation as a non-invasive, relativistic electron beam diagnostic.

The MBA is designed to accelerate a 1 kA electron beam to a final energy of 20 MeV within a 1.0 m major radius, 15 cm minor radius, toroidal vacuum chamber. In addition to the conventional betatron magnetic field with axial B_z and radial B_r components, the modified betatron utilizes a strong toroidal B_θ guide field as well as strong focusing provided by an $l = 2$ twisted quadrupole (stellarator) winding.[25]

The spectrum of synchrotron radiation emission from the modified betatron is influenced strongly by the relativistic orbit around the major axis, and the transverse beam dynamics which includes a fast electron gyro-motion about the toroidal field, an intermediate gyro-motion produced by the stellarator field, and the slow poloidal drift resulting from the interaction between the strong focusing gradients and the ring image fields. Figure 1 shows the transverse motion of a single electron obtained by numerical integration of the beam centroid equations. The beam is injected at the position $z = 0, R - R_0 = 8$ cm, where $R - R_0$ is the radial displacement off the minor axis. A poloidal electric field

(2 kV/cm) was included in the code. In the absence of this field, the beam returns to the injection position after a single poloidal orbit rather than spiraling toward the minor axis.

To obtain the differential frequency spectrum for the modified betatron electron trajectory, the radiated electric fields were calculated using numerical methods, and the frequency content determined by fast Fourier transform. The calculations neglect the influence of beam plasma dielectric effects, which is valid provided $\omega^2 \gg \omega_p^2$, where ω is the angular frequency of emission and ω_p is the electron plasma frequency. For typical MBA parameters, this condition is easily satisfied. Furthermore, it is assumed that the total radiated power is given by the superposition of single particle emission spectra. This assumption is valid provided collective effects do not lead to coherent emission in the frequency range of interest.

II. Numerical Calculation of the Radiated Spectrum

It can be shown[26] that the radiated energy per unit solid angle per unit frequency of an accelerated charge q can be expressed as the square of the Fourier transform of the time dependent radiated power per unit solid angle in the time frame of the observer, namely

$$\frac{d^2I}{d\Omega d\omega} = 2\left(\frac{1}{\mu_0 c}\right) |\,\mathrm{FT}\,[R\mathbf{E}(t)]\,|^2\,, \tag{1}$$

where FT denotes the Fourier transform. The electric field $\mathbf{E}(t)$ is the radiation component of the total electric field and can be expressed (MKS units)

$$\mathbf{E}(\mathbf{r},t) = \frac{q}{4\pi\epsilon_0}\left[\frac{\mathbf{n}\times\{(\mathbf{n}-\boldsymbol{\beta})\times\dot{\boldsymbol{\beta}}\}}{(1-\mathbf{n}\cdot\boldsymbol{\beta})^3 cR}\right]_{ret}, \tag{2}$$

where R is the distance between the charge and the observer, $\mathbf{n}$ is the corresponding unit vector, and $\boldsymbol{\beta}$ is the normalized relativistic velocity. In Eqn. 2, the position, velocity, and acceleration of the charge are evaluated in the *retarded* time frame t' of the particle.

The trajectory of a single electron located at the centroid of a cylindrical beam is determined by a numerical simulation code (STEL1_MAP) which 'pushes' the electron parameters from one time step to the next under the influence of the applied magnetic fields, the beam self-fields and their images on the conducting chamber wall[27]. The image fields are the cylindrical fields with first-order toroidal corrections,[8] and the beam is assumed to be a rigid hoop of electrons with toroidal velocity. At each time step t' in the particle frame, the value of the position ρ, 4-velocities $\gamma v_r, \gamma v_z, \gamma v_\theta$, and the energy γ are calculated for a point on the hoop. For a particular observation point $\mathbf{r}$, an array is generated which contains the cartesian components of the RHS of Eqn. 2.

The electric fields in the lab frame $R\mathbf{E}(t(i))$ are found by generating, at each time step, the value of labtime $t(i)$ that corresponds to each retarded (simulation) time t' according to the prescription $t(i) = t'(i) + R(t'(i))/c$.

Figure 2 shows the resultant array of Doppler-shifted values $R\mathbf{E}(t(i))$ plotted as a function of the labtime $t(i)$ for a 0.6 MeV electron orbiting over one period about the major axis. In (a) the transverse velocity is zero (purely circular orbit), and in (b) the electron moves with a small transverse velocity ($\beta_\perp \sim 0.1$) in a 3000 G toroidal field. In effect, the fast electric field variation associated with the electron gyro-orbit about B_θ is 'modulated' by the illumination pulse which results from the curvature of the electron orbit around the major axis.

The differential frequency spectrum is calculated by fast Fourier transform using a VAX/VMS utility program (RFFTF) which requires that the array of transform points be equally spaced in terms of the conjugate variable (in this case, time). Accordingly, a linear interpolation of the array $R\mathbf{E}(t(i))$ is performed over a set of labtime values $t(j)$

which are uniformly spaced and sufficiently dense to accurately reproduce the temporally compressed waveform.

As the electron energy increases during acceleration, the modulation pulse width (Fig. 2.) decreases more rapidly than the Doppler-shifted period of fast oscillations. Consequently, the characteristic frequencies associated with the orbit curvature increase, and the effect of the fast oscillations on the frequency content is reduced as shown in the sequence of Figure 3. It is assumed that the horizontal polarization is parallel to the midplane. Vertical polarization is perpendicular to both the horizontal direction and the vector from the electron to the observer.

At low energy ($\sim$ 1 MeV), the frequency of the spectral peak is in very good agreement with the Doppler-shifted cyclotron frequency calculated for an electron moving along a helical trajectrory in a uniform magnetic field.[15,28] The Doppler shifted cyclotron frequency ω_D is given by

$$\omega_D = \frac{\omega_{0\theta}}{1-\beta_\theta} , \tag{3}$$

where $\omega_{0\theta} = eB_\theta/\gamma m$ is the relativistic cyclotron frequency, and the radiation is observed along the direction of the magnetic field as the electron approaches with velocity $\beta_\theta c$. However, the MBA radiation spectrum is elliptically rather than circularly polarized, and contains a significant amount of lower-frequency content due to off-axis emission introduced by the curvature of the orbit. For beams located very near the minor axis, the additional poloidal motion produced by the stellarator fields has a negligible effect on the frequency content in the radiated spectrum.

At high energy (e.g. Fig. 3(c)), the radiation becomes strongly polarized in the plane of the major orbit with the characteristic frequency signature as predicted by the limiting

case of purely circular motion about the major axis.

At intermediate electron energy, the differential spectrum contains a mix of frequency components resulting from the cyclotron motion about the toroidal field and the illumination time associated with the curvature of the major radius. In this energy range, the curvature of the 'fast' gyro-orbit becomes comparable to that of the orbit around the major axis, and the net electron trajectory produces a frequency signature that is less predictable than either of the two limiting cases.

III. Description of the Experiment

In the experiment, low-level, incoherent radiation is monitored continuously during the beam lifetime in the frequency bands 26 to 29 GHz and 36 to 39 GHz using high gain heterodyne receivers. The temporal response of the radiation in each band was studied as a function of the beam current, the applied toroidal field, and the change in electron energy during acceleration. A schematic plan view showing the spatial orientation of the vacuum chamber, observation viewport, the detection system, and radiated rf power lobe for a beam centered on the minor axis is illustrated in Fig. 4.

A. Detectors

The heterodyne receivers, shown schematically in Fig. 5, each consist of a conical feed horn, Gunn diode local oscillator, balanced mixer (Millitech Corp.), +35 db, intermediate frequency (*IF*) amplifier (Miteq Co.), and *IF* detector.

A combination video amplifier and wideband line driver circuit was designed and implemented to provide a moderately high input impedance ($\sim$ 1 kΩ) amplification stage for the *IF* detector and a high-speed, low impedance output capable of driving a 50 Ω cable

and digitizer input. The measured amplifier gain is 15 db over a frequency range of 10 Hz to 70 MHz, and the circuit risetime response to a square wave input is less than 8 ns.

To calibrate the receivers, the conical feed horns were removed, and an rf signal was applied using a calibrated millimeter wave sweep signal generator (Hewlett Packard model 8690B) operating in the K_a band frequency range. The frequency-resolved output signal was measured on an oscilloscope trace and compared to the time-averaged incident power measured using a calibrated thermistor type sensor (Hewlett Packard type 432B). Excluding the losses through the acrylic port cover and the conical feed horns, the sensitivity of each of the detectors was measured to be 400 mV/μW averaged over the bandwidth ($\sim$ 3 GHz) of the receiver.

Signal losses associated with the conical feed horns and port cover were determined empirically. A section of waveguide in the receiver calibration circuit was removed and replaced with two horns configured as a transmitter/receiver pair. The power collecting efficiency of this antenna circuit was assumed to be the product of the emitting/collecting efficiency of the individual horns. Absorption/reflection losses through the port cover were determined by inserting a sample of the port cover material between the antennae, and noting the reduction in detected power. The combined effect of a single conical feed horn and port cover is an approximate 50% reduction of the incident signal transmission to the active components in the heterodyne receivers. Thus, the corrected scale factor used for the radiation measurements is actually 0.5 times the receiver sensitivity (400 mV/μW) or 200 mV/μW.

B. Shielding

The heterodyne receivers were designed to detect radiated power on the order of 0.5

to 1.0 μW/kA which corresponds to a measured signal in the range of 50 to 100 mV for a 0.5 kA beam. The low intensity of radiation created a number of problems regarding signal processing and electromagnetic noise immunity. Minimizing the length of waveguide used to transmit the incident radiation required that the receiver electronics be located near the MBA torus. Consequently, extensive shielding and power supply filtering was required to reduce the background electromagnetic noise generated by the injector pulse ($\sim 10^9$ Watts), and field coupling from the VF electromagnets.

The local oscillator, *IF* amplifier, and wideband amplifier for each receiver were electrically isolated, and individually battery powered to prevent ground loops. Each of the receivers was enclosed in a machined 1/4 inch thick aluminum rf box, fitted with coaxial inputs for the power and signals, and capacitive filtering was installed inside each box at the coax connection and at each of the detector input power 'pigtail' connections.

The components were housed in a steel enclosure which was electrically isolated from the signal ground and from the modified betatron structure. The antenna waveguides were brought into the enclosure through machined aluminum channels which were insulated from the waveguide by a thin (0.005 cm) layer of Kapton (Dupont) tape. The video output signals were transmitted to a remote, shielded diagnostic room using coaxial 50 Ω cables which were completely enclosed within a shielded conduit (also isolated from the signal ground), electrically connecting the detector enclosure to the outer shield of the screen room. Topologically, the signal cable conduit, the detector enclosure, and the machined waveguide input connections form an extended 'bulge' in the shielded surface of the diagnostic screen room.

As a result, background noise was reduced to less than 50 mV at injection and was

undetectable for times greater than a few microseconds. The shielding effectiveness was tested by blocking the horn inputs and monitoring the detector outputs in the presence of the applied fields, and an injected beam.

IV. Experimental Results and Discussion

Initially, a series of shots was taken at a fixed toroidal field for different values of trapped ring current. The receiver waveguide polarization was then changed and the shots repeated with the same experimental parameters. Radiation measurements were obtained in this manner for trapped current up to 500 A at toroidal fields in the range of about 1.9 to 3.5 kG.

The *evolution* of radiated power during acceleration was predicted by generating the spectra for a large number of simulation runs, each having slightly different energy, over the entire energy range of interest. For each spectral 'snapshot', the frequency-integrated power in each detector band was calculated, and the value of $\beta_\perp$ for each run was adjusted according to the relativistic magnetic moment[29]

$$\mathrm{M} = \frac{p_\perp^2}{2m_e B_{0\theta}} = \text{const} \ , \tag{4}$$

where, for $B_{0\theta} \gg B_z$, $p_\perp = \gamma m_e v_\perp$ is the relativistic momentum normal to the $B_{0\theta}$ magnetic field lines. The resulting energy evolution of integrated power is related to the elapsed time by the temporal dependence of the accelerating B_z field which is approximately linear during the early part of the field pulse. A typical result, shown in Fig. 6 was constructed from nineteen simulation runs, each of which varied in energy by 0.25 MeV. The plot clearly shows an increase in the detected power as the spectral peak associated with the Doppler-shifted cyclotron frequency moves into the frequency band of the het-

erodyne receiver. At lower toroidal field, the peak associated with the cyclotron frequency is broader, and occurs at higher energy consistent with the decrease of $\Omega_{0\theta}$. In addition, the 'high-power' emission associated with the orbit about the major axis is the dominant characteristic for horizontal polarization at a beam energies above about 2.5 Mev.

A. Polarization Dependence and Scaling with Trapped Current

Figure 7 shows a typical digitizer trace of the time resolved power radiated into the frequency bands (a) 26 to 29 GHz and (b) 36 to 39 GHz. The radiation is horizontally polarized and the value of the toroidal guide field is 3500 G. As predicted by simulation, the peak of the signal occurs when the injected beam has been sufficiently accelerated so that the Doppler-shifted cyclotron frequency is upshifted into the detection range of the heterodyne receiver. The amplitude of the peak corresponds to a detected power of about 0.42 μW, and the beam energy at 600 μs is approximately 12 MeV.

The amplitude of the measured cyclotron peak is plotted as a function of the trapped beam current for vertically and horizontally polarized radiation in Fig. 8. The beam current was determined from an oscilloscope display of the passively integrated Rogowski probe signal, and the uncertainty in the measured current (approximately 25 A) is due primarily to the resolution of the amplitude on the oscilloscope trace. As expected, the measured power appears to scale linearly with trapped ring current which is consistent with the assumption of incoherent emission. The best linear fit to the data ensemble was calculated with the result 460 $\pm$ 91 mV/kA and 237 $\pm$ 40 mV/kA respectively for vertically and horizontally polarized signals. The corresponding measured power is 8.5 ($\pm$ 1.4) x 10^{-15} and 16.4 ($\pm$ 3.2) x $10^{-15}\mu$W/electron which is in very good agreeement with the average of the predicted values. However, in contrast to the simulation code, the data

show no significant correlation between the amplitude of the peak and the magnitude of the toroidal field. Simulation results indicate that the peak power tends to increase with the toroidal field and the magnitude of the transverse velocity. Though the reason for the discrepancy in the measured data has not been confirmed, it is possible that beams injected in a higher toroidal field are born and trapped with proportionally lower transverse velocity.

For the first 200 μs, the relative intensity of the vertical and horizontal polarization components are also in very good agreement with the simulation predictions. However, in contrast to the predicted spectrum, the horizontal component of detected power begins to decay after a few hundred microseconds which, in most cases, is commensurate with the onset of x-rays produced by electron loss to the chamber wall. A likely cause for the signal decay is the continuous loss of beam current during the x-ray pulse coupled with motion of the beam centroid off the minor axis. The combination of the highly collimated radiation and the relatively small cross section of the antennae prevents the detection of radiation if the beam (or individual electrons) moves off the minor axis by more than about 5 cm.

B. Frequency Upshift During Acceleration

Shot to shot comparison of the measured time-resolved signals with the predicted temporal response requires the tedious assembly of many simulation runs, with varied injection energy, toroidal field, rate of acceleration, and initial transverse velocity. Since the occurrance of the peak in the predicted spectrum corresponds closely to the Doppler shifted cyclotron frequency given by Eqn. 3, a simple verification of the mechanism was obtained by analyzing the *variation* of ω_D with γ.

Equation 3 can be rewritten in terms of the non-relativistic cyclotron frequency $\Omega_{\theta 0}$,

the electron energy γ, and the transverse velocity factor $\beta_\perp$ in the following way

$$\omega_D = \frac{\Omega_{0\theta}}{\gamma - \sqrt{\gamma^2 - 1 - (\gamma\beta_\perp)^2}} \,. \tag{5}$$

A plot of the variation of the Doppler-shifted cyclotron frequency with beam energy is shown in Fig. 9 for several different values of $\gamma\beta_\perp$. Over a range of a few hundred keV, the variation of ω_D with energy is nearly linear, and the slope is weakly dependent on the value of $\gamma\beta_\perp$. For example, at 2.8 kG, an energy change of 0.335 MeV is required to increase the Doppler-shifted cyclotron frequency from 27.5 to 37.5 GHz when the value of $\gamma\beta_\perp$ is 0.3. Thus, it is possible, in principle, to determine the value of the quantity $\gamma\beta_\perp$ for a specific value of toroidal field, by knowing two closely spaced values of frequency ω_{D1},ω_{D2} and the energy change $\Delta\gamma$ which separates them. The actual beam energy at each of the frequencies ω_{D1} and ω_{D2} is then easily obtained by inverting Eqn. 5 to solve for the energy γ in terms of ω_D and $\gamma\beta_\perp$.

For high ($\sim$ 3 kG) toroidal fields, ω_D is approximately equal to the value of the heterodyne frequency at the time corresponding to the half-power point on the rising edge of the signal. Therefore, the energy gain between the values of ω_D corresponding to the heterodyne frequencies 27.5 and 37.5 GHz is given approximately by the product of the rate of change of energy and the time between the occurance of the half-power points in the measured signals.

The energy gain per turn is obtained from the product of the rate of change of the magnetic field measured at the orbit radius and the value of the betatron flux condition expressed as the ratio of the average magnetic field $\langle B_z \rangle$ over the orbit radius to the local field B_{0z} at the position of the beam. In the process to maximize beam trapping

and to investigate the cause of beam loss, several different flux conditions (2:1, 1.9:1, and 1.55:1) were tested by controlling the amount of current flowing to a set of auxiliary coils. Knowing the flux condition for a particular coil configuration, it was possible to determine the energy gain per revolution during acceleration.

Using this procedure, the electron energy and transverse velocity were calculated for a number of shots at each of the betatron flux conditions. To check the results, the energy obtained by the radiation time shifts were compared to the energy inferred from the value of the equilibrium vertical field at the same time. The few percent space charge correction was neglected. Since the analysis is based on the energy (time) shifts between the ocurrance of a specific frequency, namely the Doppler-shifted cyclotron frequency, it was possible to analyze only those shots which exhibited a well defined peak for both the 27.5 and 37.5 GHz detectors, and for which the peak occured late enough in time so that the rising edge of the 27.5 GHz detector signal was clearly discernable. In general, low toroidal field shots (less than 3 kG) were unacceptable for energy analysis because of the broadening of the spectral peak at higher electron energy.

Figure 10 shows a plot of the measured energy versus the value obtained from the single particle equilibrium field B_{z0} for 2:1 and 1.9:1 flux conditions. The plot shows the data fit using a linear regression for each of the flux conditions as well as the ideal case ($E_{measured} = E_{predicted}$) for comparison. At the 2:1 flux condition, the electron energy determined from the radiation time shift is in very good agreement with the value obtained from the local vertical magnetic field. As the flux condition is lowered, the 'measured' energy tends to decrease with respect to the matching value, which is consistent with the corresponding decrease in the accelerating electric field.

Though the mean 'detected' energy agrees quite well with the corresponding equilibrium field value for the 2:1 flux condition, the uncertainty, even for the best shots, ranges from about 7 to 12 % . The most significant source of error is the measurement of the elapsed time between the onset of the Doppler-shifted cyclotron frequency ω_D in the two fixed-frequency bands. It would be extremely difficult to improve the measurement using the existing apparatus, although a more accurate measure of the onset of ω_D could be obtained by incorporating several smaller bandwidth frequency channels in order to map-out the frequency response at any given time. However, the reduced signal in each band may require additional amplification and significantly improved noise reduction.

Typical values of $\gamma\beta_\perp$ resulting from the time shift analysis ranged from about 0.3 to 0.5, which corresponds to $\beta_\perp$ in the range 0.14 to 0.25 for an initial beam energy of 0.6 MeV. Though the error associated with this measurement is high ($\sim$ 20 to 30%), this is consistent with recent anode damage pattern results indicating that the injected beam has a transverse velocity component which may be as high as 0.25c.

V. Conclusions

The phenomenon of incoherent synchrotron radiation from a relativistic electron beam has been studied numerically and experimentally for electron trajectories in the magnetic field configuration of the NRL modified betatron accelerator. As a result of these studies, a reliable technique for predicting the synchrotron radiation emission for complicated 'periodic' motion of a charged particle has been developed, revealing a distinctive, spectral signature produced by the characteristic transverse 'fast' mode of the modified betatron.

Measurements of the temporal evolution of the radiation in two fixed frequency bands show that, at low electron energy, the polarization, amplitude, scaling with trapped beam

current, and the temporal evolution of measured radiation during acceleration are in very good agreement with the predicted single particle spectrum.

By utilizing appropriate rf and magnetic field shielding techniques, incoherent radiation produced by low current (less than 0.1 kA) beams can be resolved easily, even in a relatively high noise environment.

It was possible to neglect self-field effects on the cyclotron frequency because of the trapped current was relatively low ($\sim$ few hundred amps). Recently, the trapped current in the MBA has been increased to greater than a kiloamp, and continued studies of the radiated spectrum at moderate beam energy may require the inclusion of both space charge effects and the electron energy distribution. Efforts are underway to extend the diagnostic capability of the technique to include the characteristic emission frequencies associated with a higher energy (e.g. 20 MeV) electron ring.

References

*. Work supported by ONR and SPAWAR.

†. Berkeley Research Associates, Inc., Springfield, VA.

1. J. Golden, L.K. Len, A.V. Deniz, J. Mathew, T. Smith, P. Loschialpo, J.H. Chang, D. Dialetis, S.J. Marsh, and C.A. Kapetanakos, 7th International Conference on High-Power Particle Beams, Karlsruhe, Germany, Vol. I, p. 221 (1988).

2. H. Ishizuka, R. Prohaska, A. Fisher, and N. Rostoker, Beams '88, 7th Int'l Conf. on High-Power Particle Beams, Karlsruhe, Germany, Vol. II, p. 857.

3. S. Humphreys, Jr., and L.K. Len, Proceedings of the 1987 IEEE Particle Accelerator Conference, Washington, DC, p.914.

4. V. Bailey *et al*, Proceedings of the 1987 IEEE Particle Accelerator Conference, Washington, DC, p.920.

5. W.K. Tucker *et al*, Proceedings of the 1987 IEEE Particle Accelerator Conference, Waashington, DC, p. 957.

6. P. Sprangle and C. A. Kapetanakos, J. Appl. Phys. **49**, 1 (1978).

7. N. Rostoker, Comments Plasma Phys. **6**, 91 (1980).

8. C. A. Kapetanakos, P. Sprangle, D. P. Chernin, S.J. Marsh, and I. Haber, Phys. Fluids **26**, 1634 (1983).

9. D. W. Kerst, Phys. Rev. **60**, 47 (1941).

10. D. W. Kerst and R. Serber, Phys. Rev. **60**, 53 (1941).

11. C. A. Kapetanakos, L. K. Len, T. Smith, J. Golden, K. Smith, S. J. Marsh, D. Dialetis, J. Mathew, P. Loschialpo, and J. H. Chang, Phys. Rev. Let. **64**, 2374 (1990).

12. S. C. Chen and T. C. Marshall, Phys. Rev. Letters **52**, 425 (1984).

13. D. Chernin and B. Levush, J. Appl. Phys. **61**, 2737 (1987)

14. T. Smith, Ph.D. Thesis, University of Maryland (1990)

15. C. A. Kapetanakos, R. E. Pechacek, D. M. Spero, and A. W. Trivelpiece, Phys. Fluids **14**, 1555 (1971).

16. C. A. Kapetanakos and A. W. Trivelpiece, J. Appl. Phys. **42**, 4821 (1971).

17. C. P. DeNeef, R. E. Pechacek, and A. W. Trivelpiece, Phys. Fluids **16**, 512 (1973).

18. S. F. Nee, A. W. Trivelpiece, and R. E. Pechacek, Phys. Fluids **16**, 502 (1973).

19. F. J. Stauffer, D. A. Boyd, and A. W. Trivelpiece, Phys. Lett. A **57**, 401 (1973).

20. S. M. Mahajan, C. R. Oberman, and R. C. Davidson, Plasma Phys. **16**, 1147 (1974).

21. R. C. Davidson, Phys. Fluids **18**, 1143 (1975).

22. F. J. Stauffer, Ph.D. thesis, University of Maryland (1976).

23. G. D. Tsakiris and R. C. Davidson, Phys. Fluids **20**, 436 (1977).

24. G. D. Tsakiris, D. A. Boyd, D. A. Hammer, R. C. Davidson and A. W. Trivelpiece, Phys. Fluids **21**, 2050 (1978).

25. C. W. Roberson, A. Mondelli and D. Chernin, Part. Accel. **17**, 79 (1985).

26. J. D. Jackson, *Classical Electrodynamics*, Wiley (1962), Chap. 14.

27. original simulation program written by A. V. Deniz, SAIC.

28. G. Bekefi, *Radiation Processes in Plasmas*, Wiley (1966), Chap. 6.

29. T. G. Northrop, *The Adiabatic Motion of Charged Particles*, Interscience Publishers (1963), Chap. 1.

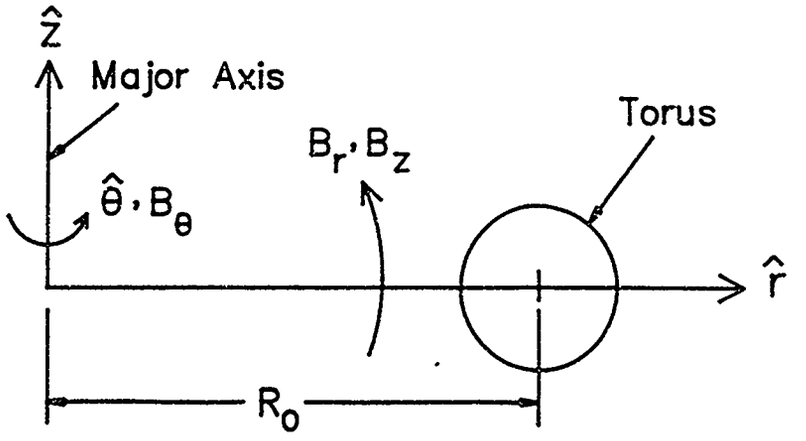

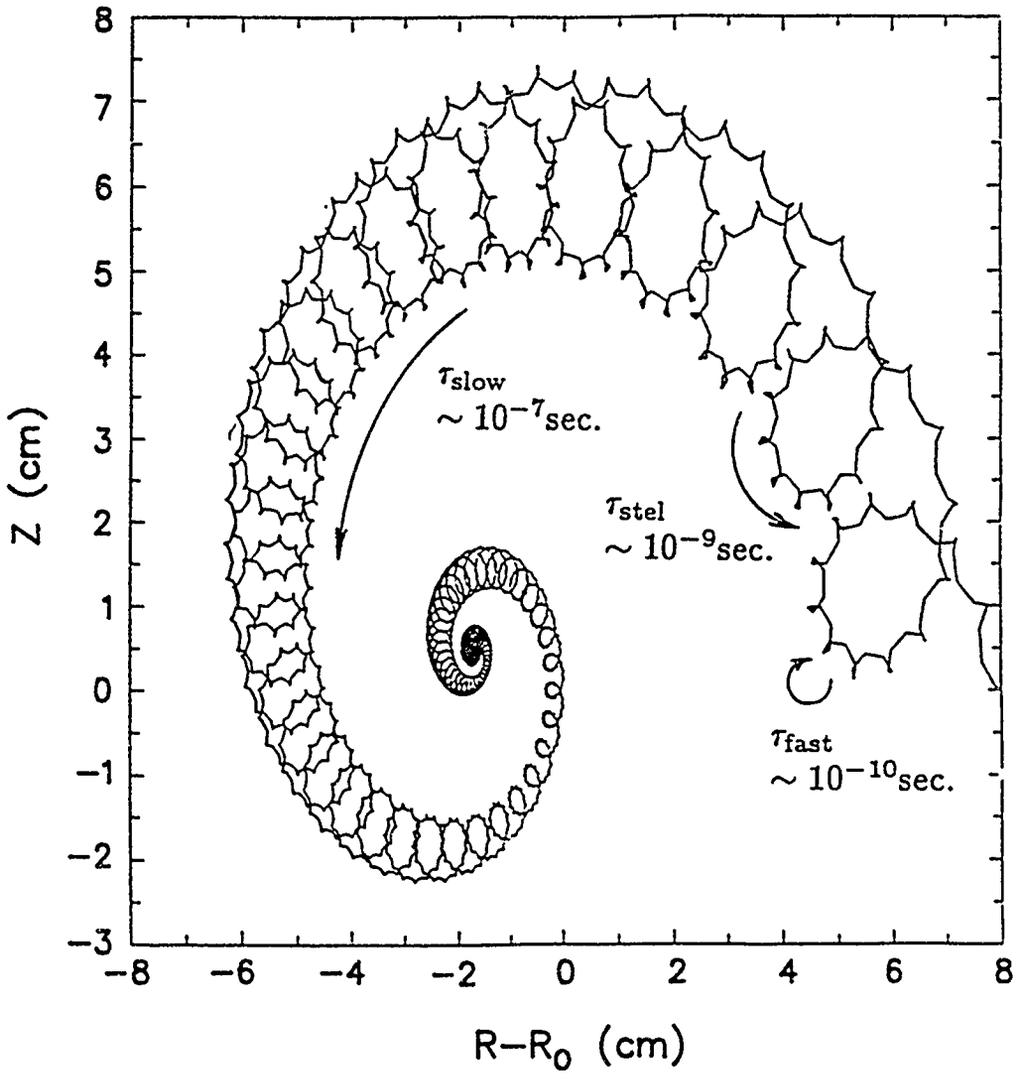

Fig. 1 — Computer simulation of the transverse motion of the beam centroid in the modified betatron

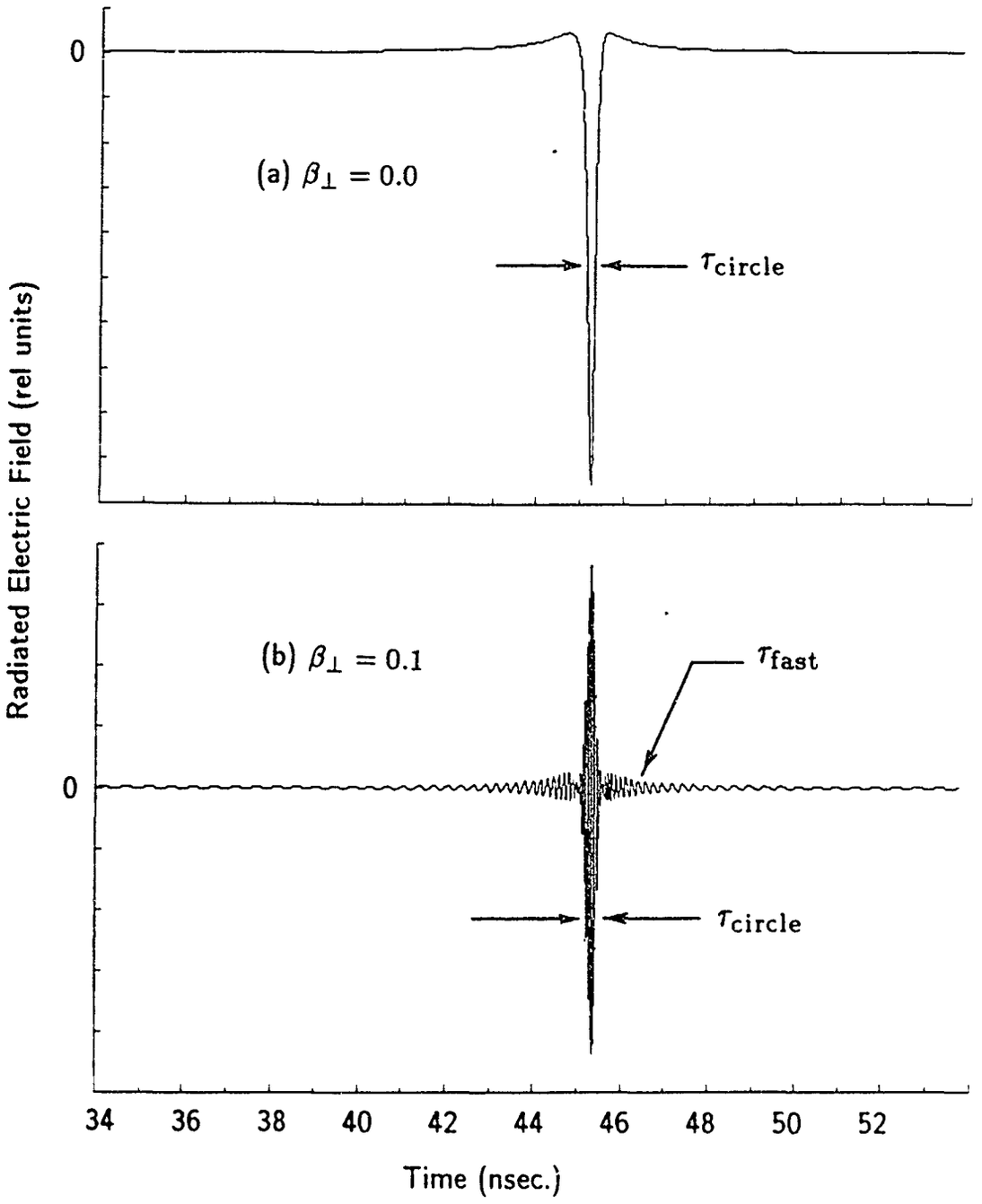

Fig. 2 – Radiated electric fields for a 0.6 MeV electron orbiting over one period around the major axis. In (a), the electron has no transverse velocity. In (b), the electron is given a 'small' transverse velocity.

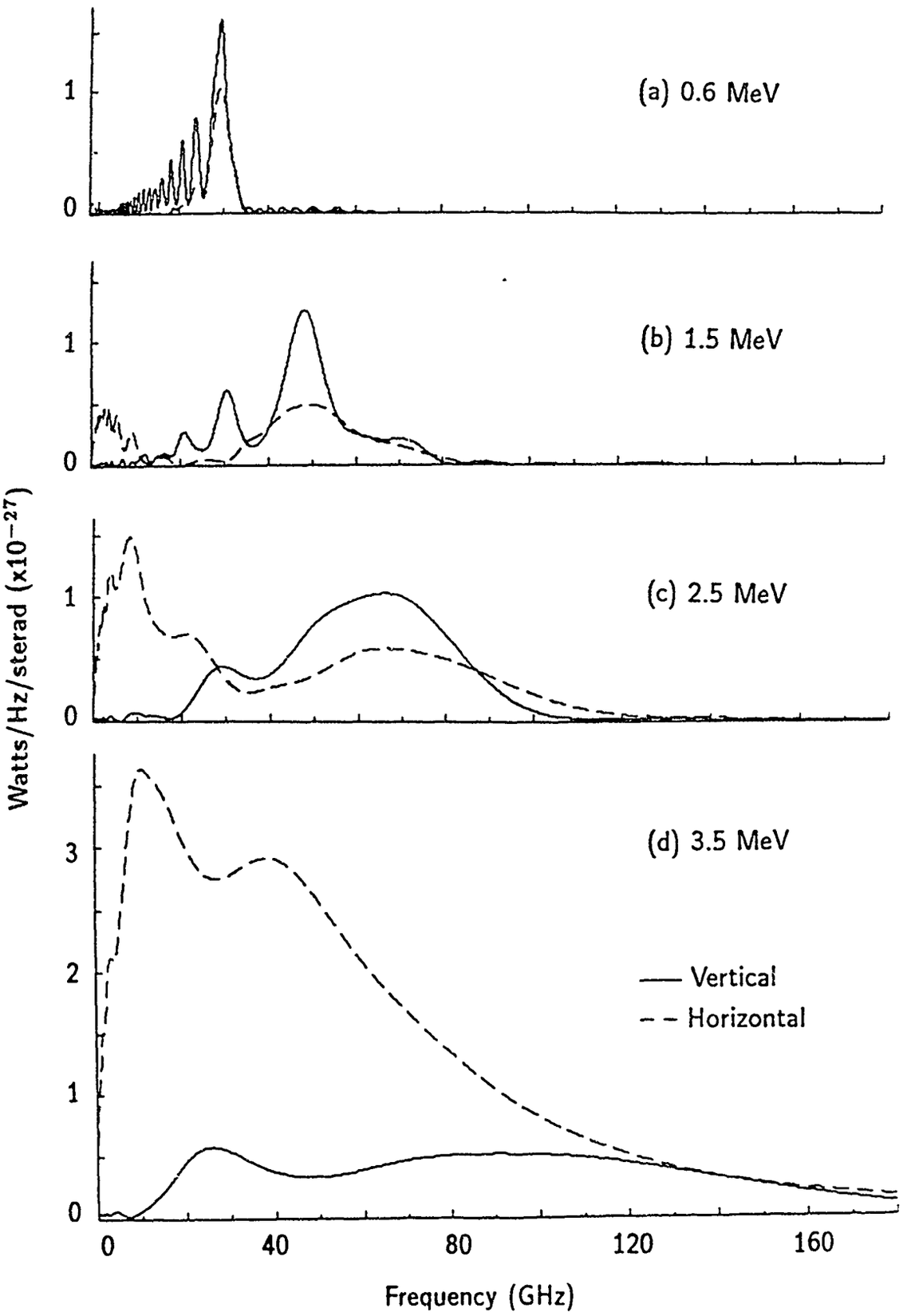

Fig. 3 — Evolution of single particle emission spectrum with increasing electron energy

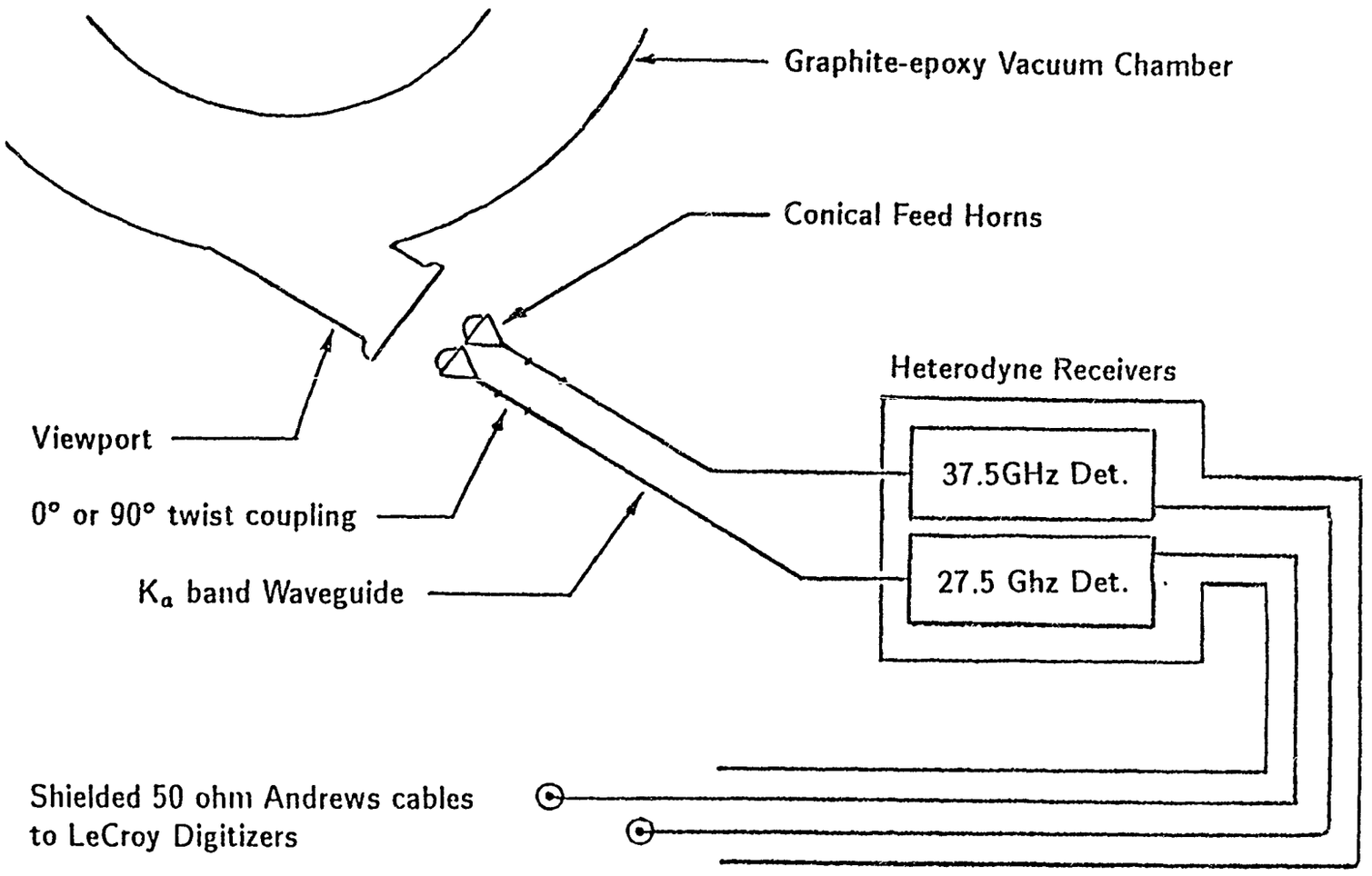

Fig. 4 — Plan view of the radiation diagnostic components

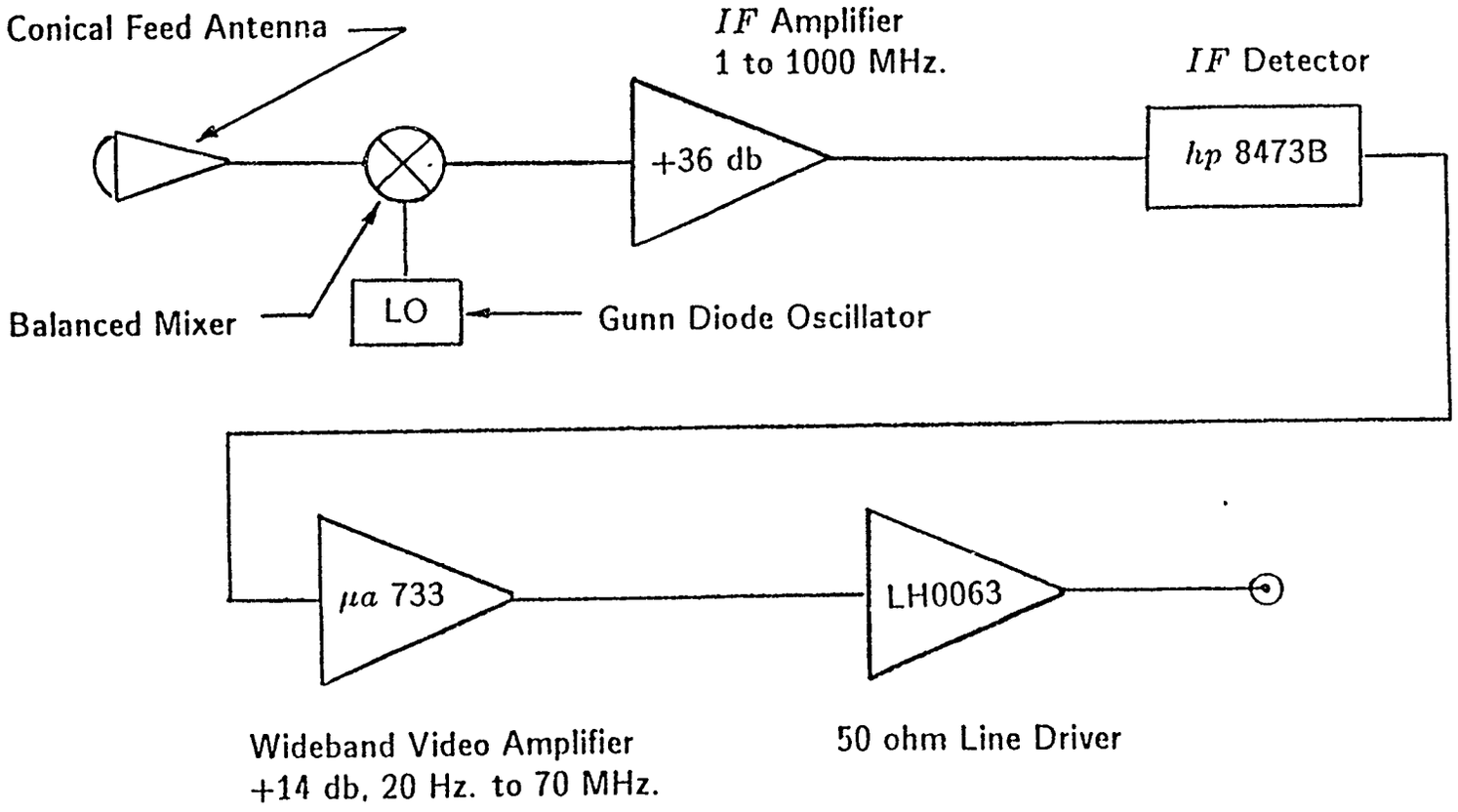

Fig. 5 — Typical heterodyne receiver channel

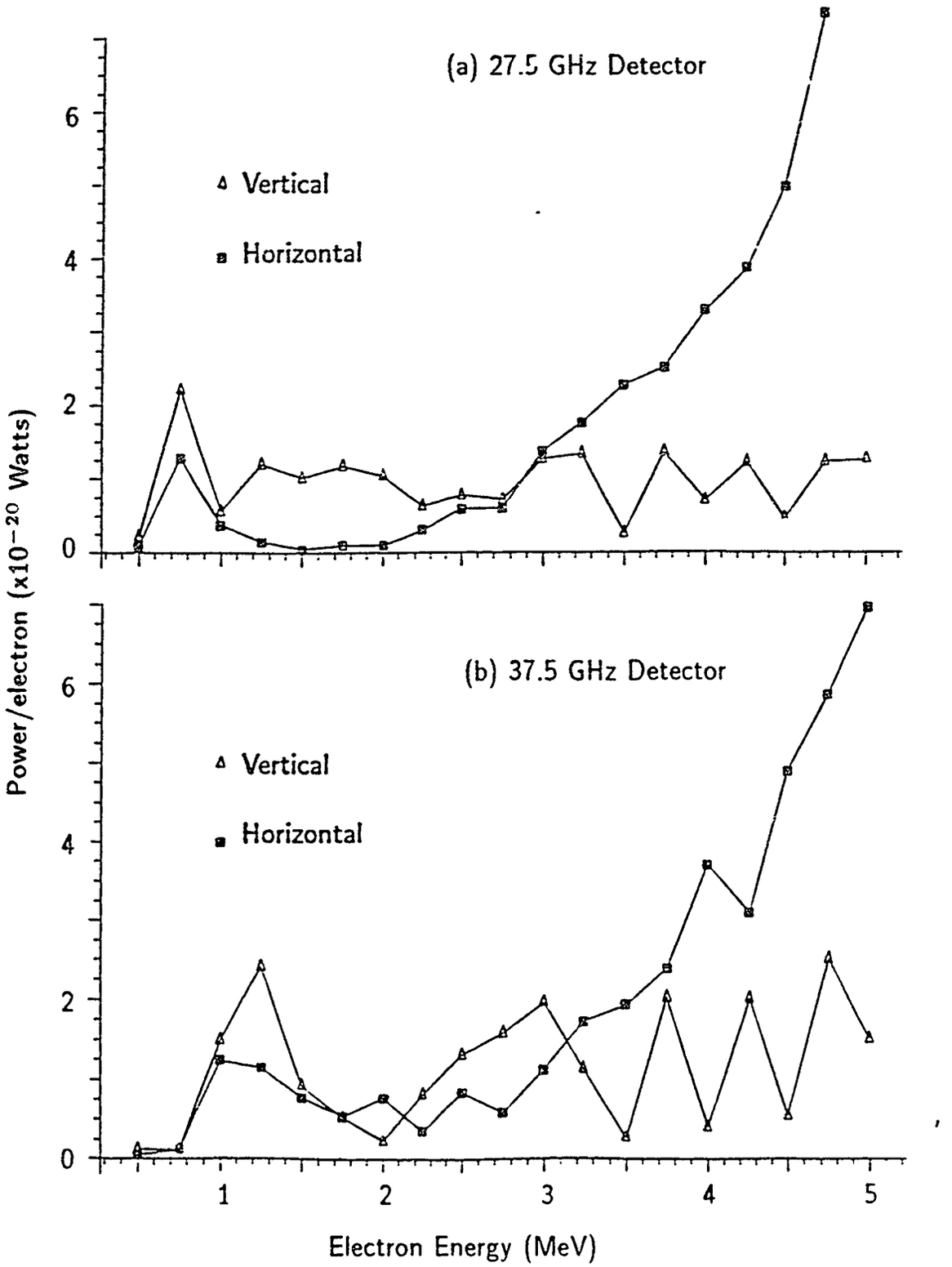

Fig. 6 — Simulation of the energy-resolved power in the (a) 27.5 GHz and (b) 37.5 GHz detectors. The initial value of $\beta_\perp$ was 0.2, the injection energy was 0.5 MeV, the stellarator current with approximately 20 Ka, and the toroidal guide field was 2.8 kG.

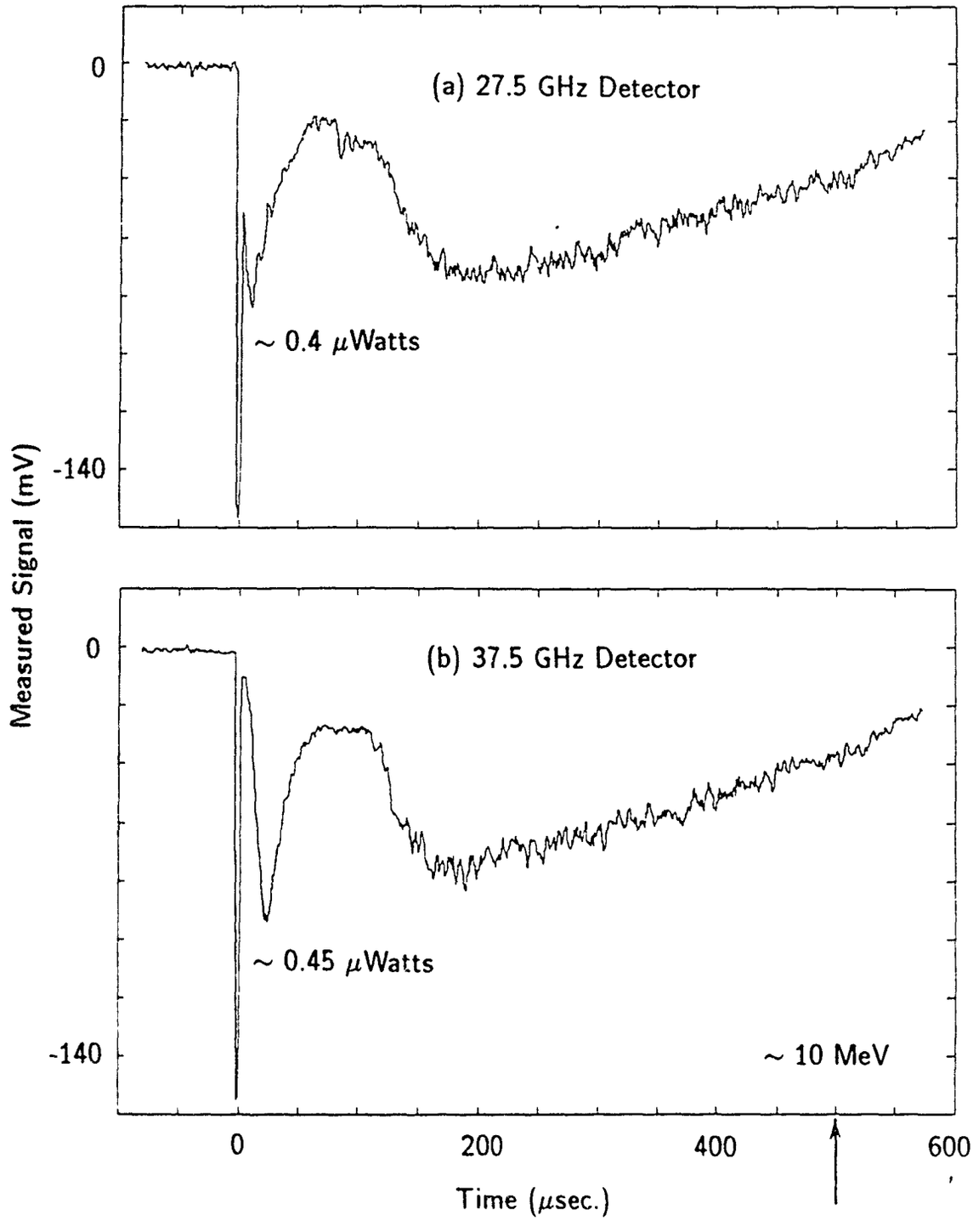

Fig. 7 — Time resolved power radiated into the (a) 27.5 GHz and (b) 37.5 GHz detectors. The radiation is horizontally polarized, and the value of the toroidal field is 3.5 kG.

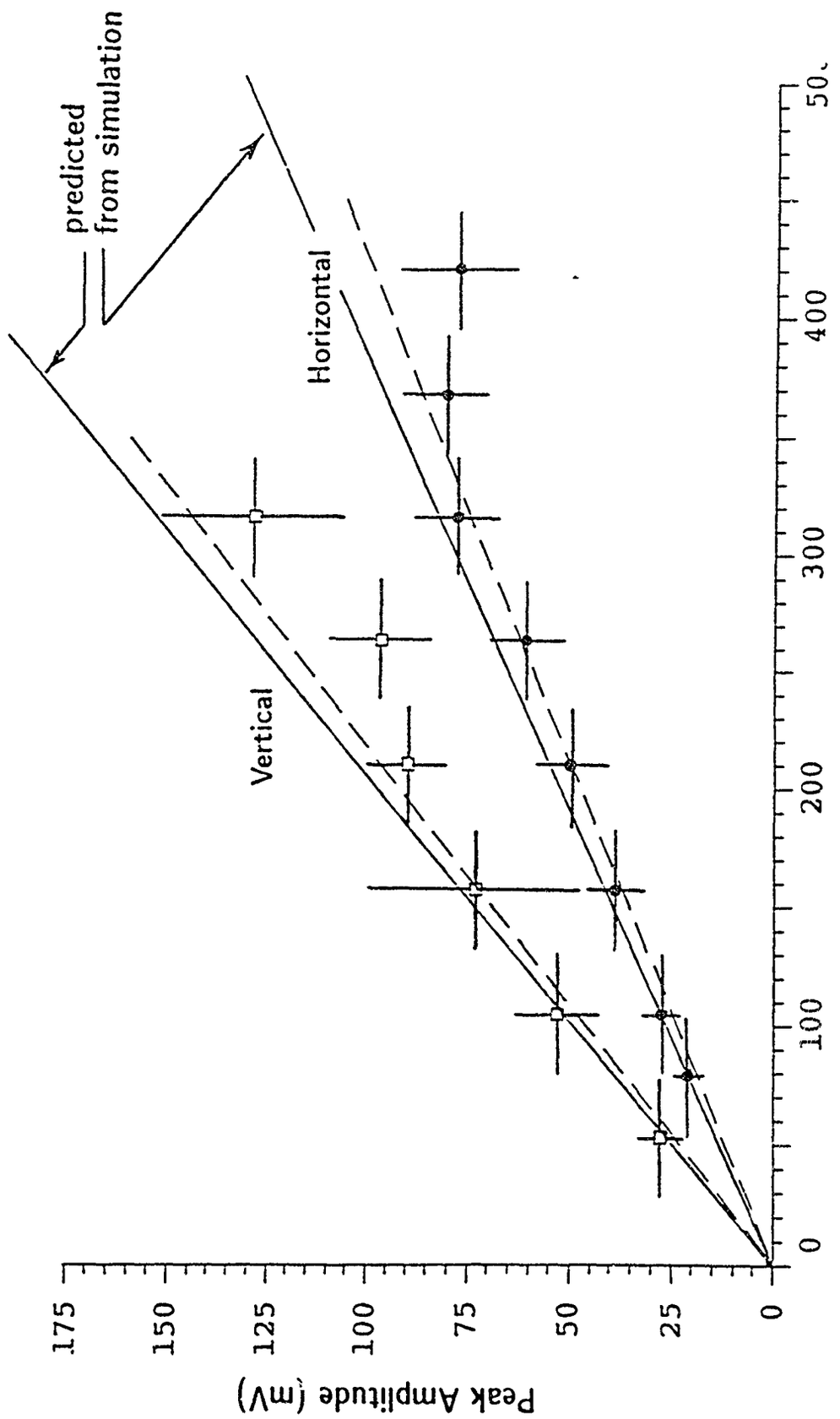

Fig. 8 — Variation of peak signal amplitude with trapped current for vertically and horizontally polarized radiation.

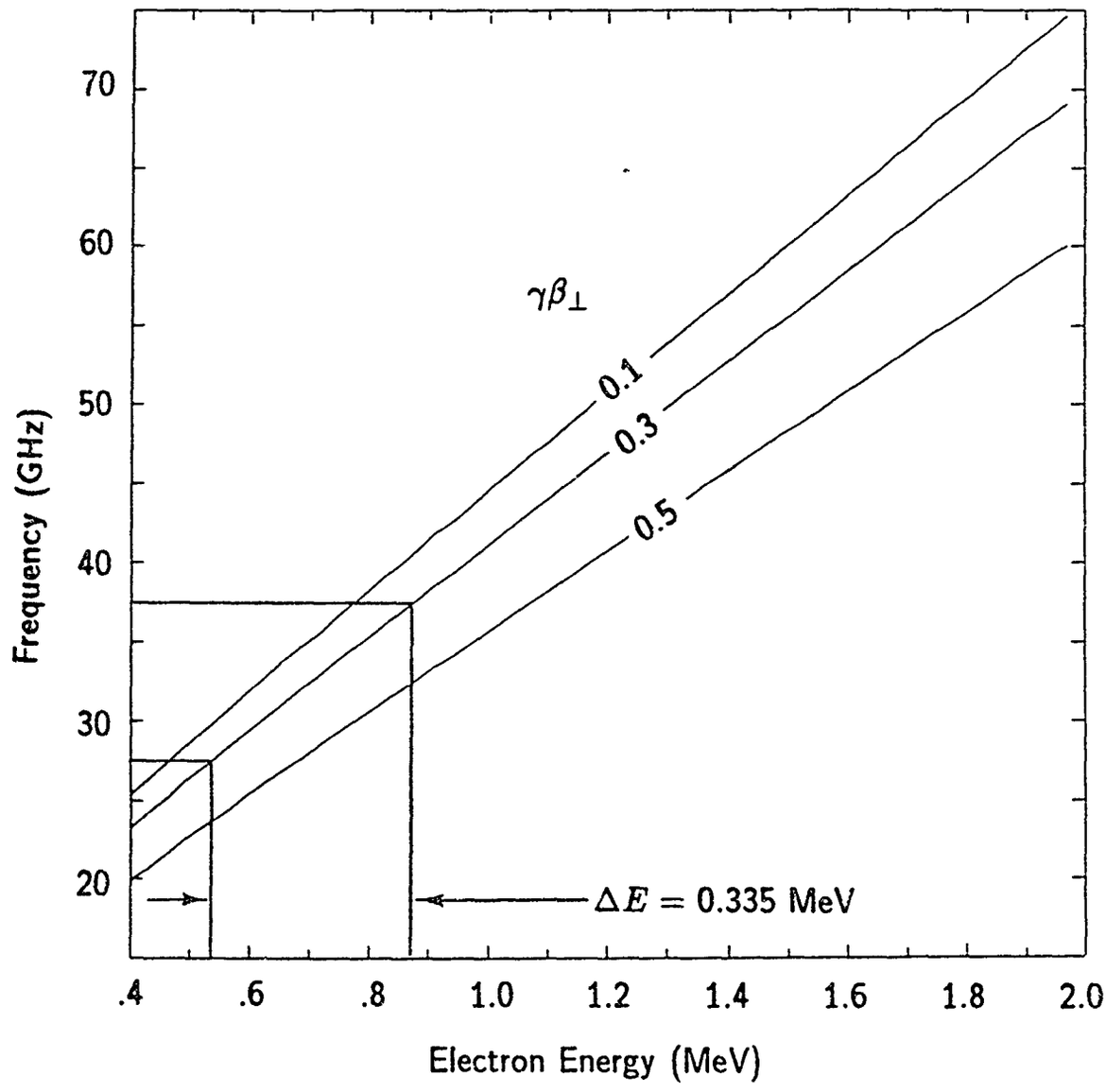

Fig. 9 — Variation of the Doppler shifted cyclotron frequency with electron energy as a function of the quantity $\gamma\beta_\perp$. For $\gamma\beta_\perp = 0.3$, an energy change of 0.335 MeV is required to increase the Doppler-shifted cyclotron frequency from 27.5 to 37.5 GHz.

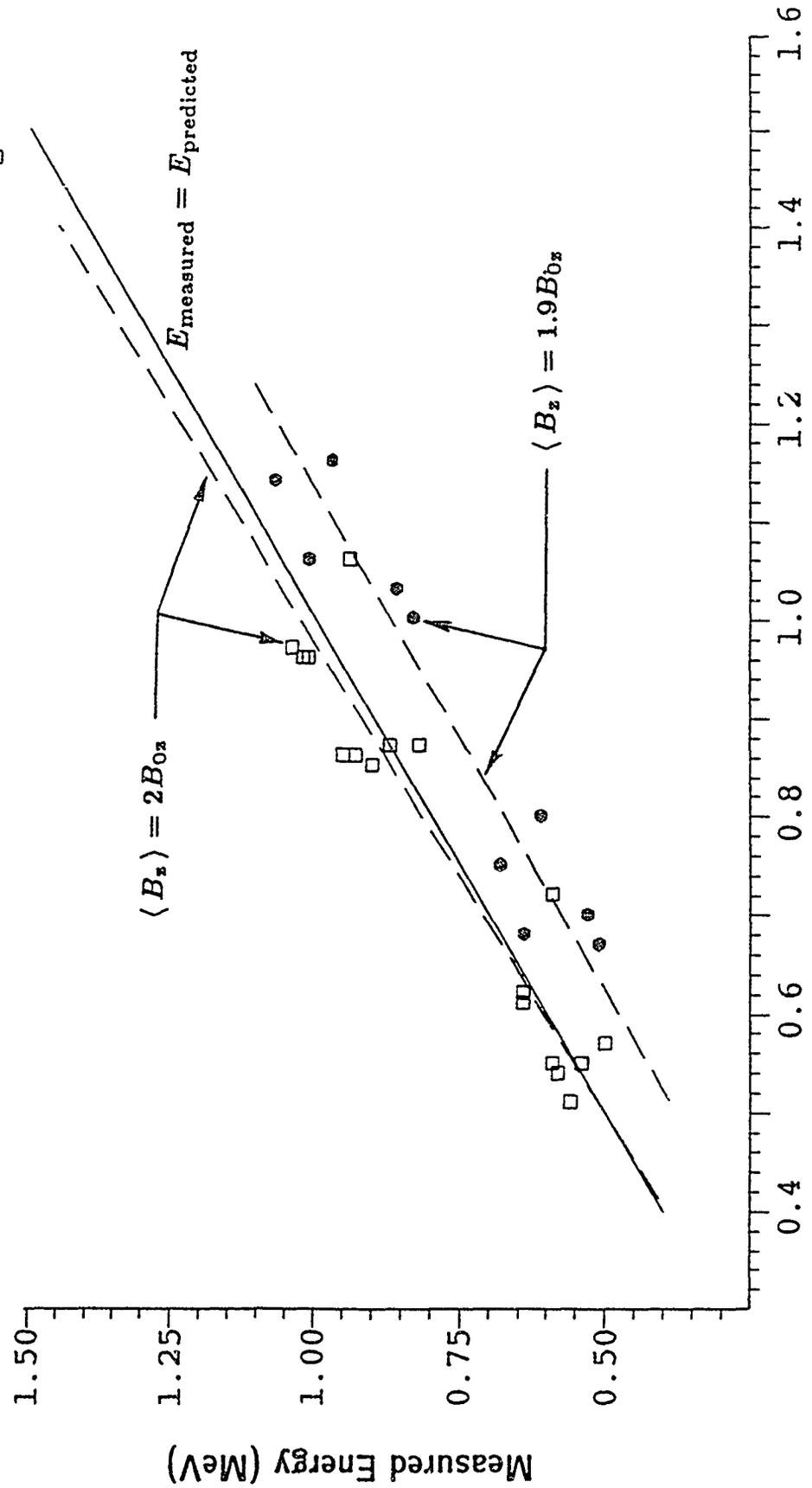

Fig. 10 — Comparison of the electron energy calculated from the detector time shift and the value obtained for the equilibrium vertical field B_{0z}